Transactions of the Materials Research Society of Japan 29 [8] 3427-3430 (2004)

Preparation of Nanocrystalline Diamond in a Low Pressure Inductively Coupled Plasma

Katsuyuki Okada, Koji Kimoto, Shojiro Komatsu, and Seiichiro Matsumoto
National Institute for Materials Science, 1-1 Namiki, Tsukuba, Ibaraki 305-0044, Japan
Fax: 81-29-852-7449, e-mail: okada.katsuyuki@nims.go.jp

A 13.56 MHz low pressure inductively coupled $CH_4/CO/H_2$ plasma has been applied to prepare nanocrystalline diamond particles with several hundred nm in diameter. The low loss region of electron energy loss spectra exhibits a bulk plasmon peak at 33 eV and a surface plasmon peak at 23 eV. The plasma diagnostics with a Langmuir probe reveals that the electron impact dissociation of CO brings about the decrease in electron density, leading to the simultaneous increase in electron temperature and plasma potential.
Key words: nanocrystalline diamond, low pressure inductively coupled plasma, electron energy loss spectroscopy, Langmuir probe, electron energy distribution function

1. INTRODUCTION

A microwave plasma has been most commonly used for the plasma-enhanced chemical vapor deposition (PE-CVD) of diamond films, in which the conventional pressure of deposition is of the order of several ten Torr. A CH_4/H_2 mixture, in which the CH_4 content ([CH_4]) is usually less than 5 %, leads to μm size polycrystalline diamond films. On the other hand, recent plasma dry processes (e.g., deposition, coating, etching) require a wide area and high density plasma at low pressures (<1 Torr) [1]. An electron cyclotron resonance (ECR) plasma was first developed to meet these conditions. Subsequently, a helicon-wave excited plasma and a surface-wave excited plasma were employed. It was found [2] that the plasma density of an inductively coupled plasma (ICP) after the transition from a low density E-discharge to a high density H-discharge reaches 10^{12} cm^{-3}. Thus the ICP has been recognized to be eminently suitable for use in a dry process. Since the growth conditions of diamond in a low pressure ICP have not yet optimized, it is required to establish the synthesis of diamond in a low pressure ICP and to find out the optimum growth condition.

Amorphous and nanostructured carbon materials have attracted considerable attention in the last 20 years since the PE-CVD of diamond was developed, followed by fullerenes and carbon nanotubes [3]. From applied perspectives, they are being extensively studied for electron emitters, cold-cathode sources, hard low-friction coatings, etc. From fundamental perspectives, on the other hand, the structure of these materials contains both three-fold coordinated (sp^2-bonded) and four-fold coordinated (sp^3-bonded) carbon atoms. Nanocrystalline diamond films also have drawn remarkable attention [4] because they have a low coefficient of friction and low electron emission threshold voltage. The small grain size (approximately 5-100 nm) gives films with valuable tribology and field emission properties, being compared with those of conventional polycrystalline diamond films. Furthermore, applications for MEMS devices, MESFETs, electrochemical electrodes, biochemical devices have been proposed by taking advantage of these excellent properties [5-7].

Since the authors have first reported the effect of CO on diamond deposition in a low pressure ICP [8], Teii et al followed the procedure with the same gas mixture ($CH_4/CO/H_2$) [9]. In this study, a 13.56 MHz low pressure $CH_4/CO/H_2$ ICP has been utilized for the synthesis of nanocrystalline diamond. The characterization with electron energy loss spectroscopy (EELS) and the plasma diagnostics with a Langmuir probe are described in this article.

2. EXPERIMENT

The schematic view of the low pressure ICP-CVD system is illustrated in Figure 1. The detailed description and deposition procedures were reported previously [10]. To be brief, a low pressure ICP was

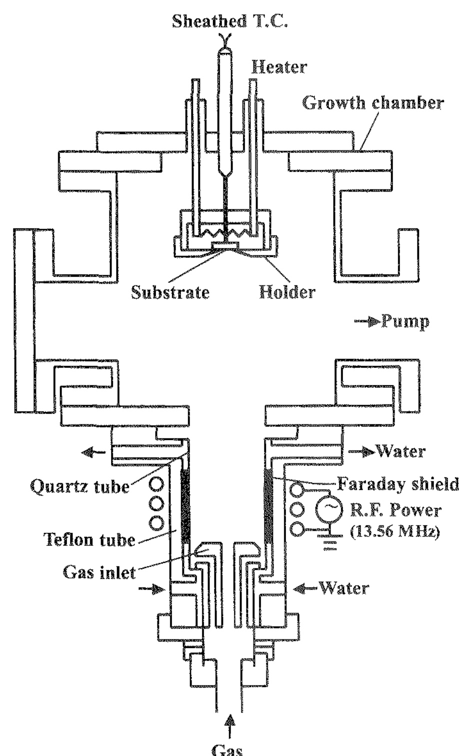

Fig. 1. Schematic description of the low pressure inductively coupled rf plasma CVD system.

generated in a growth chamber by applying 13.56 MHz rf powers of 1 kW to a three-turn helical antenna. The flow rates of CH_4 and H_2 were kept at 4.5 and 75 sccm, respectively, whereas the flow rate of CO ([CO]) was varied between 0, 1.0, 5.0, and 10 sccm, respectively. The total gas pressure was accordingly varied from 45 to 50 mTorr. Silicon (100) wafers (10 mm in diameter) were used as a substrate. The substrate temperature was kept at 900 ℃. The deposition duration was 2 h.

EELS measurements [11] were carried out by using a post-column energy filter (GATAN, GIF2002) equipped with a transmission electron microscope (TEM; Hitachi HF-3000) at 297 keV.

A Langmuir probe was utilized to measure plasma parameters {plasma potential (V_p), electron temperature (T_e), and electron density (N_e)} and electron energy distribution functions (EEDFs). A probe was inserted through one of the side flanges of the chamber as shown in Fig. 1 [12]. The probe tip was a cylindrical tungsten wire, which was 0.19 mm in radius and was 10 mm in length. The rf fluctuations of the plasma potential were compensated by self-resonant inductors [13]. The reference probe, which was a stainless-steel casing mounted on the probe shaft, automatically compensated for the plasma-ground sheath impedance, fluctuations in the plasma sheath impedance, plasma potential shifts, and low frequency noise [13].

3. RESULTS AND DISCUSSION

Figure 2 shows the SEM photographs of the resultant deposits on a Si(100) substrate. Fig. 2(a), (b), (c) and (d) correspond to [CO]=0, 1.0, 5.0, and 10 sccm, which are labeled as sample A, B, C, and D, respectively. The morphology of sample A was two-dimensional platelet-like as shown in Fig. 2(a), and crystal facets were not clearly seen. When CO was added to a CH_4/H_2 plasma, particles with the size of 200-300 nm in diameter as well as platelet-like deposits appeared as shown in Fig. 2(b). With the increase of [CO], only particles were deposited as shown in Fig. 2(c) and (d). The background of the particles was the substrate. The diameters of the particles were 200-700 nm. The average diameters of the particles are increased with increasing [CO]. The detailed observation reveals that the particles consist of small particles of about several ten nm in diameter, and that the sizes are almost same regardless of increasing [CO]. Since carbon atoms derived from the dissociation of CO make the supersaturation degree of carbon large with increasing [CO], the number of encountered particles is expected to increase.

The previous TEM observations have revealed [10] that the two-dimensional platelet-like deposits consist of disordered microcrystalline graphite, whereas the particles are composed of only diamond nanocrystallites. The high-resolution TEM images clearly show that each particle is composed of small particles of about several ten nm in diameter. The X-ray diffraction pattern for the sample D exhibits the diffraction peaks of diamond (111) and (220) planes [14]. The crystallite size was estimated to be approximately 20 nm from the full width at half maximum (FWHM) of the diamond peaks by using the Scherrer's equation. It is consistent with the TEM observations.

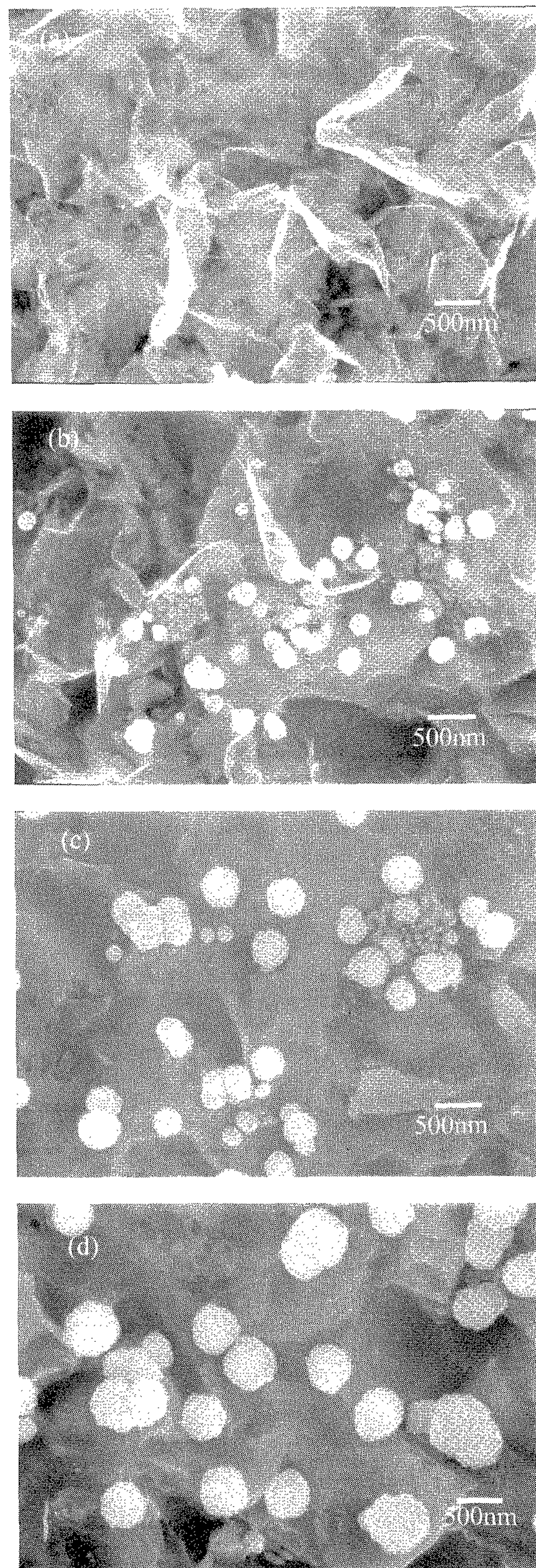

Fig. 2. SEM micrographs of the obtained deposits; (a) [CO]=0 sccm, (b) [CO]=1.0 sccm, (c) [CO]=5.0 sccm, (d) [CO]=10 sccm.

Figures 3(a) and 3(b) show the low loss region of EEL spectra of a nanocrystalline diamond particle in sample D and a graphite-like platelet in sample A, respectively. The low loss region, extending from 0 to ~50 eV, corresponds to the excitation of electrons in the outermost atomic orbitals and reflects the solid state character of the sample. The low loss region is dominated by collective, resonant oscillations of the valence electrons known as plasmons [15]. In Fig. 3(a), the peak at 33 eV is assigned to the bulk plasmon, E_B of diamond, and the shoulder at 23 eV is attributed to the surface plasmon, E_S of diamond. The E_S is almost equal to the $E_B/\sqrt{2}$, which is consistent with the previous report on diamond [16]. It was also reported [17] that the intensity of surface plasmon peak to that of bulk plasmon peak increases with decreasing crystallite size of nanocrystalline diamond.

On the other hand, the low loss spectrum of a graphite-like platelet as shown in Fig. 3(b) consists of two peaks at 27 eV and 6 eV. The former corresponds to the main plasmon peak of graphite, and the latter to a π to π^* interband transition, which reflects the excitation of valence electrons to low-energy unoccupied electronic states above the Fermi level [15]. The whole spectrum shape is similar to that of graphite reported previously [15].

We have demonstrated the sp^2 bonding distributions in the nanocrystalline diamond particles by the π^* peak of the high loss region of the EEL spectrum [11]. The mapping of sp^2 states reveals that sp^2 bondings are localized in the grain boundaries of 20-50 nm subgrains. Thus we can say that the combination of low loss and high loss regions of EEL spectra enables one to perform extensive characterizations of nanocrystalline diamond and nanostructured carbon.

Figures 4(a)-(c) show the variation of the V_p, the T_e, and the N_e of a $CH_4/CO/H_2$ plasma with [CO]. While the V_p and the T_e are increased with increasing [CO], the N_e is decreased with increasing [CO].

Figures 5 shows the EEDFs of a $CH_4/CO/H_2$ plasma as a function of [CO]. There is a hump at ~6 eV in the EEDF of a CH_4/H_2 plasma as shown in Fig. 5(a). In the CH_4 vibrational excitation cross sections, $\sigma_v(1, 3)$ and $\sigma_v(2, 4)$ have a peak at ~6 eV [18]. The hump can be attributed to the electric absorption of CH_4 molecule analogous to the vibrational absorption of ~4 eV electrons of the N_2 molecule [19]. The hump at ~6 eV still appears with the addition of CO as shown in Figs. 5(b) and (c), and the spectrum shape remains almost the same feature. The inclinations below 6 eV become slow with increasing [CO], which means the Te increases with increasing [CO]. It is consistent with the result of Fig. 4(b).

The electron impact dissociation of CH_4 and CO occurs in a $CH_4/CO/H_2$ plasma in the following reactions [20, 21]:

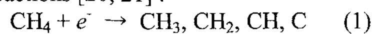

$$CH_4 + e^- \rightarrow CH_3, CH_2, CH, C \quad (1)$$

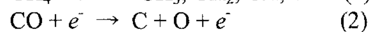

$$CO + e^- \rightarrow C + O + e^- \quad (2)$$

$$CO + e^- \rightarrow C + O^- \quad (3).$$

After the dissociation of CO by the reactions (2) and (3), the by-product of O atoms are lost, which leads to an increase of OH radicals produced by the reactions with H_2 and CH_4. The reactions involve a simultaneous

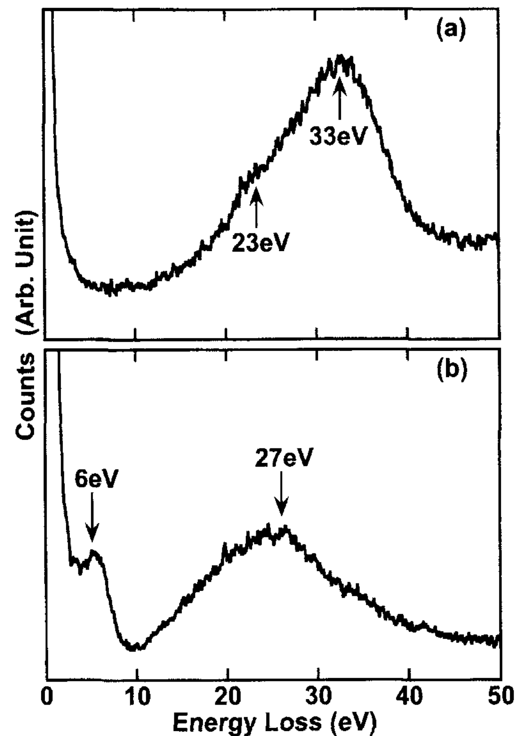

Fig. 3. Low loss spectra of (a) nanocrystalline diamond and (b) graphite-like platelet.

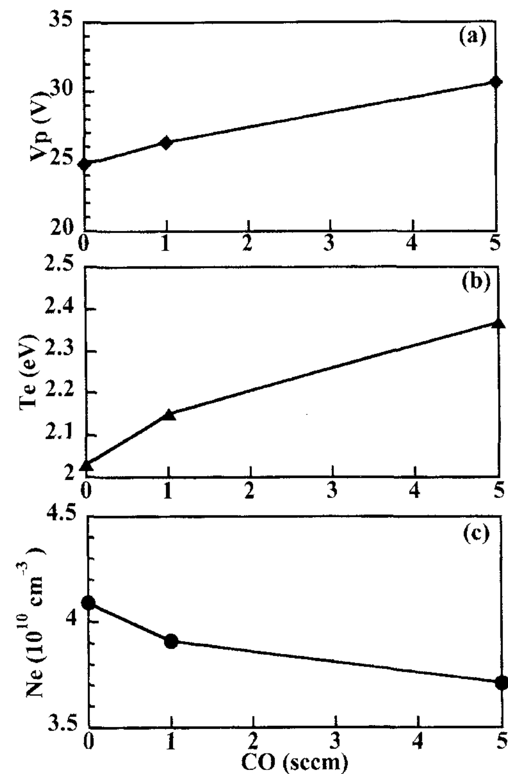

Fig. 4. Variation of the plasma parameters of $CH_4/CO/H_2$ plasma with [CO] content; (a) plasma potential, (b) electron temperature, and (c) electron density.

increase in H and CH_3, respectively. Subsequent reactions of OH [21] :

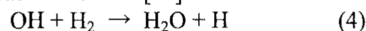
$$OH + H_2 \rightarrow H_2O + H \quad (4)$$

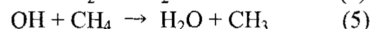
$$OH + CH_4 \rightarrow H_2O + CH_3 \quad (5)$$

also yield H and CH_3. On the other hand, C atoms dissociated from CO possibly recombine with C or H to form C_2 dimers or CH_3 radicals. CH_3 is thought to be a main precursor radical for diamond growth, and atomic hydrogen keeps the growing surface sp^3-hybridized by the abstraction of surface bonded H atoms [22]. OH radical also has a high abstraction efficiency. Therefore, the increase in H and OH by the dissociation of CO is responsible for the enhanced diamond growth. It is in agreement with the fact that the addition of CO to a CH_4/H_2 plasma produces nanocrystalline diamond particles.

The dissociation of CO also produces negative ions O^- by the reaction (3) in a $CH_4/CO/H_2$ plasma. It is therefore considered that the increase in negative ions reduces the N_e relatively to satisfy the charge balance in a plasma. The ionization threshold of CO ($CO + e^- \rightarrow C + O^-$; 9.5 eV) is much smaller than those of CH_4 ($CH_4 + e^- \rightarrow CH_3^+$; 14.3 eV, $CH_4 + e^- \rightarrow CH_2^+$; 15.1 eV) [23]. Thus high energy electrons survive in a $CH_4/CO/H_2$ plasma, which leads to the increase in T_e and V_p.

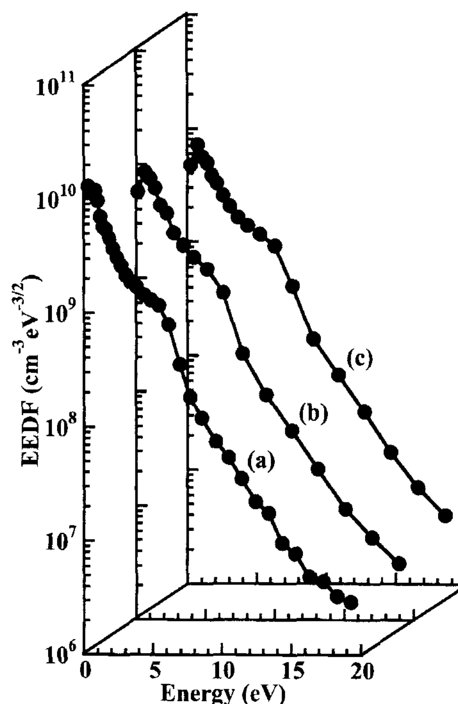

Fig. 5. Electron energy distribution functions of a $CH_4/CO/H_2$ plasma as a function of [CO]; (a) [CO]=0 sccm, (b) [CO]=1.0 sccm, and (c) [CO]=5.0 sccm.

4. CONCLUSION

Nanocrystalline diamond particles with several hundred nm in diameter were prepared in a 13.56 MHz low pressure inductively coupled $CH_4/CO/H_2$ plasma. The low loss region of EEL spectra exhibits a bulk plasmon peak at 33 eV and a surface plasmon peak at 23 eV. The plasma diagnostics with a Langmuir probe reveals that the electron impact dissociation of CO brings about the decrease in N_e, leading to the simultaneous increase in T_e and V_p. The dissociation of CO also earns the increase in H, OH, and CH_3, which are responsible for the enhanced diamond growth.

REFERENCES

[1] M. A. Lieberman and A. J. Lichtenberg, *Principles of Plasma Discharges and Materials Processing*, John Wiley & Sons, New York (1994).

[2] J. Amorim, H. S. Maciel, and J. P. Sudano, J. Vac. Sci. Technol. **B9**, 362 (1991).

[3] J. Robertson, T. A. Friedmann, and D. B. Geohegan Eds., Mater. Res. Soc. Symp. Proc. **675** (2001).

[4] D. M. Gruen, Annu. Rev. Mater. Sci. **29**, 211 (1999).

[5] J. Philip, P. Hess, T. Feygelson, J. E. Butler, S. Chattopadhyay, K. H. Chen, and L. C. Chen, J. Appl. Phys. **93,** 2164 (2003).

[6] J. A. Carlisle, J. Birrell, J. E. Gerbi, O. Auciello, J. M. Gibson, and D. M. Gruen, 8th Inter. Conf. New Diamond Sci. Tech., Melbourne, p. 129, 2002.

[7] G. M. Swain, A. B. Anderson, J. C. Angus, MRS Bull. p.56, 1998.

[8] K. Okada, S. Komatsu, and S. Matsumoto, Proc. 13th Symp. Plasma Processing, Tokyo, pp.25-28, 1996.

[9] K. Teii and T. Yoshida, Thin Solid Films **316,** 24 (1998).

[10] K. Okada, S. Komatsu, and S. Matsumoto, J. Mater. Res. **14,** 578 (1999).

[11] K. Okada, K. Kimoto, S. Komatsu, and S. Matsumoto, J. Appl. Phys. **93,** 3120 (2003).

[12] K. Okada, S. Komatsu, and S. Matsumoto, J. Vac. Sci. Technol. **A17,** 721 (1999).

[13] M. B. Hopkins, J. Res. Natl. Inst. Stand. Technol. **100,** 415 (1995).

[14] K. Okada, H. Kanda, S. Komatsu, and S. Matsumoto, J. Appl. Phys. **88,** 1674 (2000).

[15] R. Brydson, *Electron Energy Loss Spectroscopy*, Springer-Verlag, New York, (2001).

[16] S. Prawer, K. W. Nugent, D. N. Jamieson, J. O. Orwa, L. A. Bursill, and J. L. Peng, Chem. Phys. Lett. **332,** 93 (2000).

[17] S. Prawer, K. W. Nugent, D. N. Jamieson, J. O. Orwa, L. A. Bursill, and J. L. Peng, Chem. Phys. Lett. **332,** 93 (2000).

[18] W. L. Morgan, Plasma Chem. Plasma Process. **12,** 477 (1992).

[19] M. M. Turner and M. B. Hopkins, Phys. Rev. Lett. **69,** 3511 (1992).

[20] K. Teii, H. Ito, M. Hori, T. Takeo, and T. Goto, J. Appl. Phys. **87,** 4572 (2000).

[21] D. L. Baulch, C. J. Cobos, R. A. Cox, C. Esser, P. Frank, Th. Just, J. A. Kerr, M. J. Pilling, J. Troe, W. Walker, and J. Warnatz, J. Phys. Chem. Ref. Data **21,** 411 (1992).

[22] J. C. Angus and C. C. Hayman, Science **241,** 913 (1988).

[23] T. Nakano, H. Toyoda, and H. Sugai, Jpn. J. Appl. Phys. **30,** 2908 (1991).

(Received October 8, 2003; Accepted March 12, 2004)